Advective superdiffusion in superhydrophobic microchannels

Tatiana V. Nizkaya,[1] Evgeny S. Asmolov,[1,2] and Olga I. Vinogradova[1,3,4,*]

[1]*A. N. Frumkin Institute of Physical Chemistry and Electrochemistry, Russian Academy of Science,*
31 Leninsky Prospect, 119071 Moscow, Russia
[2]*Institute of Mechanics, M. V. Lomonosov Moscow State University, 119991 Moscow, Russia*
[3]*Department of Physics, M. V. Lomonosov Moscow State University, 119991 Moscow, Russia*
[4]*DWI – Leibniz Institute for Interactive Materials, Forckenbeckstr. 50, 52056 Aachen, Germany*

We consider pressure-driven flows in wide microchannels, and discuss how a transverse shear, generated by misaligned superhydrophobic walls, impacts cross-sectional spreading of Brownian particles. We show that such a transverse shear can induce an advective superdiffusion, which strongly enhances dispersion of particles compared to a normal diffusion, and that maximal cross-sectional spreading corresponds to a crossover between its subballistic and superballistic regimes. This allows us to argue that an advective superdiffusion can be used for boosting dispersion of particles at smaller Péclet numbers compared to known concepts of passive microfluidic mixing. This implies that our superdiffusion scenario allows one efficient mixing of much smaller particles or using much thinner microchannels than methods, which are currently being exploited.

I. INTRODUCTION

Superhydrophobic (SH) textures in the Cassie state, where the texture is filled with gas, have motivated numerous studies during the past decade [1,2]. Such surfaces are important due to their superlubricating potential [3–7]. The use of highly anisotropic SH textures with generally tensorial effective hydrodynamic slip, $\mathbf{b}_{\mathrm{eff}}$ [7–10] (due to secondary flows transverse to the direction of the applied pressure gradient [11,12]), provides new possibilities for hydrodynamic flow manipulation [10,13–15]. Recent studies have employed transverse components of flow in SH channels to fractionate large non-Brownian microparticles [16,17] or enhance their mixing [18,19]. However, we are unaware of any previous work that has addressed the issue of diffusive transport of tiny Brownian particles by generating transverse flows in SH devices.

Diffusive transport controls diverse situations in biology and chemistry [20], and its understanding is very important in many areas including such as nanoswimmers propulsion [21] or interpretation of modern nanovelocimetry experiments [22]. Dispersion of tiny Brownian particles in a cross section of a microchannel with smooth walls at low Reynolds number Re, which is relevant to many applications, is difficult since the normal diffusion (characterized by the linear time dependence of the mean squared displacement, $\sigma^2 \propto t$) is slow compared with the convection of particles along the microchannel. Our strategy here is to enhance such a dispersion by using advective diffusion, which can be induced by generating a transverse component of flow. Transverse flow generated by herringbone patterns in the Wenzel state (when liquid follows the topological variations of the surface) has already been successfully used for a passive chaotic mixing of particles in a microchannel of thickness H comparable to its width W and at very large Péclet number, Pe [23–25]. Here we suggest that dramatic improvement of a cross-sectional dispersion

in a very wide channel, $W \gg H$, and at much smaller Pe (which is equivalent to significantly reduced particle sizes or channel thickness) could be achieved by inducing a superdiffusion, i.e., a situation, when $\sigma^2 \propto t^\alpha$ with $\alpha > 1$. Depending on the value of α one usually distinguishes between subballistic ($1 < \alpha < 2$), ballistic ($\alpha = 2$), and superballistic ($\alpha > 2$) regimes of superdiffusion [26]. The superdiffusion in a flow field has been studied by several groups for various macroscopic systems. Subballistic regime has been reported for a random velocity field [27,28], and superballistic dispersion has been predicted for turbulent [29] and for linear shear [30] flows, and for a solute transport in a heterogeneous medium [31]. Some efforts have also gone into investigating a role of confinement in the emergence of superdiffusion [32]. However, advective superdiffusion on microscales has never been predicted theoretically, nor has it been used for microfluidic applications.

The presence of an additional variable H in the system implies that diffusive behavior in a confined complex flow should be different than it would be in bulk liquid or near a single interface. Could various superdiffusive regimes be induced in microchannels with realistic parameters of the flow? How will they differ from the bulk systems if induced? What are possible implications for microfluidic mixing? These questions still remain open, and we are unaware of any previous attempts describing answers to them.

In this paper we present a general strategy for inducing an advective superdiffusion in microchannels of a high aspect ratio, $W/H \gg 1$, that can be used for boosting dispersion of Brownian particles between streams of main (forward) Poiseuille flows. To enhance the mixing (homogenization) of particles over the cross section of the channel we use secondary (transverse) shear flows generated in microchannels decorated by crossed identical SH stripes [14] as sketched in Fig. 1. We show that such a flow configuration allows one to induce various scenarios of a superdiffusion, and argue that a crossover between subballistic and superballistic regimes provides large transverse dispersion of particles,
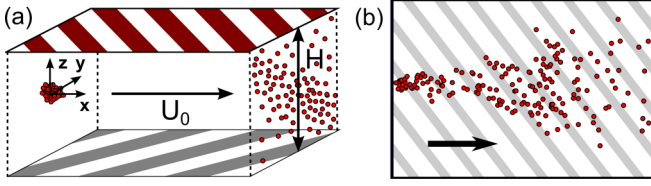
---

*oivinograd@yahoo.com

033109-1

FIG. 1. (a) Sketch of the superhydrophobic channel with identical, but misaligned striped textures at the walls. Main flow direction is from left to right. (b) Top view of particle dispersion.

which would be impossible in standard microchannels with smooth homogeneous walls or in devices, which are currently widely used as microfluidic mixers.

II. SCALING THEORY

We first present the scaling approach which we have developed to evaluate hydrodynamic dispersion in a Poiseuille flow with superimposed uniform transverse shear:

$$U_x = U_{sx} + U_0(1 - 4(z/H)^2), \quad U_y = 2U_{sy}z/H, \quad (1)$$

where $U_0 = -H^2 \nabla P / (8\mu)$ is the maximal velocity of a flow generated by pressure gradient ∇P with no-slip walls, μ is the dynamic viscosity, and U_{sx} and U_{sy} are the (positive definite) averaged forward and transverse slip velocities at channel walls located at $z = \pm H/2$. We note that the transverse shear rate is equal to $2U_{sy}/H$.

Brownian particles are injected from a point source located at $(x,y,z) = (0,0,0)$ and then advected by the flow satisfying Eq. (1). The flux of particles across channel walls is equal to zero, we neglect their inertia and focus on the diffusive regime.

Since both U_x and U_y depend only on z, particle distribution in the z direction will be governed by normal Brownian diffusion with zero average displacement. For an unbounded space we have $\langle z \rangle = 0$, $\sigma_z^2 = \langle (z - \langle z \rangle)^2 \rangle = 2Dt$, where $\langle \cdot \rangle$ denotes averaging over the ensemble of particles, and D is the diffusion coefficient. In our case diffusion is constrained by channel walls, so that sometime later particles become uniformly distributed between them:

$$\sigma_z^2 = 2Dt, \quad t \ll t_d, \quad \sigma_z^2 = H^2/12, \quad t \gg t_d. \quad (2)$$

Here we have defined the diffusion time scale, $t_d = H^2/(2D)$, as a typical time for a single particle to cross the channel in the z direction.

Particle dispersion in the y direction reflects an interplay between diffusion and transverse shear rate. Depending on t different scenarios of the particle spreading may occur. In the short time regime, i.e., for $t \ll t_d$, our shear flow could be treated as unbounded, since the spreading of particles is still unaffected by confinement. By substituting the expression for a transverse shear rate into a solution for a mean square displacement of Brownian particles in an unbounded linear shear [30] we obtain

$$\sigma_y^2 = 2Dt \left[1 + \frac{1}{3} \left(\frac{2U_{sy}t}{H} \right)^2 \right], \quad t \ll t_d. \quad (3)$$

This expression defines a second time scale $t_s = H/(2U_{sy})$, which is associated to a transverse shear.

We note that depending on the value of the Péclet number, $\mathrm{Pe} = U_0 H/D$, the ratio $t_d/t_s = U_{sy}\mathrm{Pe}/U_0$ can vary in a large interval. Two limits can now be discussed depending on the ratio t_d/t_s. When $t_d/t_s \ll 1$, which is equivalent to $\mathrm{Pe} \ll U_0/U_{sy}$, the normal Brownian diffusion of particles provides their efficient spreading in the channel since D is large. However, if $t_d/t_s \gg 1$, which corresponds to $\mathrm{Pe} \gg U_0/U_{sy}$ (or small D), the normal diffusion is slow. Therefore, below we discuss this larger Pe limit in more detail. We note that in this situation if $t \ll t_s$, the mean square displacement of particles scales as $\sigma_y^2 \propto Dt$, indicating a normal Brownian diffusion. However, for $t \gg t_s$, we deduce from Eq. (3) $\sigma_y^2 \propto Dt^3 U_{sy}^2 H^{-2}$, which suggests a superdiffusion of particles in a superballistic regime.

In the long-time regime, $t \gg t_d$, multiple rebounds of particles from the channel walls should inevitably lead to a random variation of the transverse velocity even in our directed shear flow. This situation is similar to considered in prior work [27,28] on Brownian particles in a (bulk) random velocity field, which predicted $\sigma_y^2 \propto t^{3/2}$. The characteristic velocity and length are determined by U_{sy} and H, so that dimensional analysis immediately leads to

$$\sigma_y^2 \propto D^{-1/2} U_{sy}^2 H t^{3/2}, \quad t \gg t_d. \quad (4)$$

We now summarize the different scaling expressions for σ_y^2, which determine several diffusion-advection regimes when $\mathrm{Pe} \gg U_0/U_{sy}$, and turn to dimensionless parameters:

$$\sigma_y^2/H^2 \propto \begin{cases} t/t_d, & t \ll t_s \\ (U_{sy}/U_0)^2 \mathrm{Pe}^2 (t/t_d)^3, & t_s \ll t \ll t_d \\ (U_{sy}/U_0)^2 \mathrm{Pe}^2 (t/t_d)^{3/2}, & t_d \ll t. \end{cases} \quad (5)$$

Equation (5) includes the ratio U_{sy}/U_0, which depends on the superhydrophobic texture topology only. We focus here on microfluidic applications, and therefore it is not the time, but the channel length $x = \lambda H$, that serves as a main independent parameter of the problem. So we have to reformulate Eq. (5) in terms of λ. A time required for particles to migrate along the channel is $t = \lambda H/U_m$, where U_m is a mean forward flow velocity in the locus of the assembly of particles. At $t \ll t_d$ it is equal to the velocity at the midplane of the channel, $U_m = U_0$, but at $t \geqslant t_d$ this will be the mean forward velocity in the channel, $U_m = 2U_0/3$. Note that in both cases the relationship between λH and t is linear, $t/t_d \propto \lambda/\mathrm{Pe}$. Therefore, Eq. (5) can be rewritten as

$$\sigma_y^2/H^2 \propto \begin{cases} \mathrm{Pe}^{-1}\lambda, & \lambda \ll U_0/U_{sy}, \\ (U_{sy}/U_0)^2 \mathrm{Pe}^{-1}\lambda^3, & U_0/U_{sy} \ll \lambda \ll \mathrm{Pe}, \\ (U_{sy}/U_0)^2 \mathrm{Pe}^{1/2}\lambda^{3/2}, & \lambda \gg \mathrm{Pe}. \end{cases} \quad (6)$$

In the other limit of $\mathrm{Pe} \ll U_0/U_{sy}$, a normal diffusion is expected as discussed above, so that in this case we should also get $\sigma_y^2/H^2 \propto \mathrm{Pe}^{-1}\lambda$. For a given diffusion coefficient we obtain for the superballistic regime $\sigma_y^2 \propto U_0^2 t^3 \propto U_0^{-1}$ (when the flow is too fast the migration time is too small) while for the subballistic regime we get $\sigma_y^2 \propto U_0^2 t^{3/2} \propto U_0^{1/2}$. These two scalings imply the existence of optimum U_0 and corresponding $\mathrm{Pe}_{\max}$.
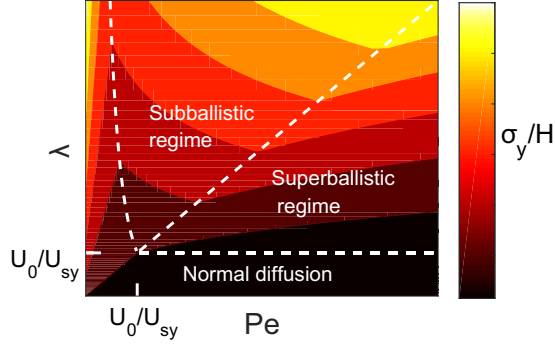
FIG. 2. Schematic representation of various diffusion regimes in a microchannel. The colorbar values ascend from bottom to top.

FIG. 3. Cross section of the fluid velocity field (u_y, u_z) at $\phi = 0.5$ and $\lambda = 0.5$. Colorbar shows the forward velocity U_x.

To illustrate this effect it is useful to divide the (λ, Pe) space into three regions of normal, subballistic, and superballistic diffusion, where the above scaling expressions for σ_y^2/H^2 approximately hold. Such a diagram is plotted in Fig. 2. The crossover loci here simply indicate that limiting solutions for σ_y^2/H^2 given by Eq. (6) coincide for different regimes of diffusion. Apart from the curve $\lambda = \text{Pe}^{3/2}(U_0/U_{sy})^2$ (separating the normal and superballistic diffusion), other crossover loci, $\lambda = \text{Pe}$ (separating the subballistic and superballistic regions) and $\lambda = U_0/U_{sy}$ (between the normal and superballistic diffusion) are straight lines. Of course, in reality at those curves, the limiting solutions for σ_y^2/H^2 cross over smoothly from one diffusion regime to another. We can now conclude that when λ is below U_0/U_{sy} only normal diffusion is expected. In other words, advective superdiffusion cannot be generated without large slip at SH walls. When λ is above U_0/U_{sy} three regimes can be attained depending on the value of Pe. A very small Péclet number will lead to a normal diffusion, but at larger Pe one can induce a subballistic and at very large Pe a superballistic regime. Figure 2 also immediately shows that the maximal spreading is attained at the crossover between subballistic and superballistic regimes. This means that it happens when the time required for particles to migrate forward to a given cross section and to diffuse to the channel walls are comparable.

III. SIMULATION METHOD

We model a motion of Brownian particles, i.e., a situation when inertia is neglected and Langevin equations are reduced to first order

$$\dot{\mathbf{x}} = \mathbf{u}(\mathbf{x}) + \mathbf{r}(t), \qquad (7)$$

where $\mathbf{x}$ is a particle position, $\mathbf{u}(\mathbf{x})$ is the velocity field of a fluid and $\mathbf{r}(t)$ is a random velocity component with a correlation time much smaller than other time scales in the system. To discretize the equation we introduce a time grid $\{t_k\}$ with the step Δt and keep the random component $\mathbf{r}_k = (r_x, r_y, r_z)$ constant over the time step $[t_k, t_k + \Delta t]$ with random variables $r_{x,y,z}$ taken from the Gaussian distribution with zero average and dispersion u_r.

To validate that we model a dispersion of particles correctly we first measure their diffusion coefficient. We integrate the equation of particle motion for an ensemble of 500 particles released at $\mathbf{x}_0 = (0,0,0)$ in a velocity field involving a uniform

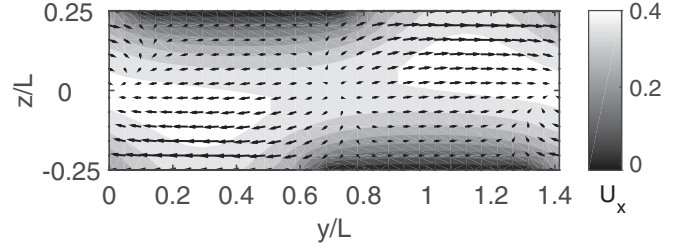$\mathbf{u} = (U_0, 0, 0)$ and a random component $\mathbf{r}_k = (0, r_y, r_z)$, and then measure the dispersion of particle positions $\sigma_{y,z}(t)$ at $t \leqslant T$. We then fit the dispersion curves using the standard scaling $\sigma_{y,z}^2(t) = 2D_{y,z}t$. The diffusion coefficient is the same in all directions, $D_z = D_y = D$, and depends on the time step Δt and the dispersion u_r as $D = D^* u_r^2/(2\Delta t)$, where D^* is a renormalization coefficient. We have computed the values of D^* using $U_0 = 1$, $T = 10$, several u_r in the range from 0.05 to 0.5, and Δt varying from 0.01 to 0.1. In all the cases, the simulations give $D^* = 1$, which confirms that the scaling holds in the whole range of our parameters.

The velocity field in the SH channel is calculated using the solution of Stokes equations valid at $H/L \simeq 1$ [14]:

$$\mathbf{u} = \langle \mathbf{u} \rangle + \mathbf{u}_1 + \mathbf{u}_2. \qquad (8)$$

Here $\langle \mathbf{u} \rangle = (U_x, U_y, 0)$ is the averaged flow profile defined by Eq. (1), and $\mathbf{u}_1$, $\mathbf{u}_2$ are perturbations with zero mean over the cell volume due to heterogeneous slippage at the lower and upper walls, respectively. The perturbation fields $\mathbf{u}_1$ and $\mathbf{u}_2$ are obtained using Fourier series with 50 harmonics [33].

In simulations of superdiffusive regimes we also use an ensemble of 500 particles. To calculate the contribution of the fluid velocity field, $\mathbf{u}(\mathbf{x})$, the equation of motion, Eq. (7), is solved using fourth order Runge-Kutta method with the time step $\Delta t = 0.01 L/U_0$. In these simulations bounce-back boundary conditions are applied at the channel walls.

IV. RESULTS AND DISCUSSION

In order to assess the validity of the above scaling approach we now model a situation when the transverse shear is created by SH walls [14], as sketched in Fig. 1. Specifically, we consider a pressure-driven flow between two parallel SH surfaces separated by the distance H, which are decorated with identical periodic stripes of a period L and a fraction of the gas area ϕ. We assume SH surfaces to be flat with no meniscus curvature, so that the gas area is characterized by a local slip length b only, and solid area has no-slip. The lower and the upper wall textures are misaligned by an angle $\pi/2$, and we align the x axis and the pressure gradient with this angle bisector. The Reynolds number $\text{Re} = \rho U_0 H/\mu$, where ρ is the fluid density, is considered to be small, i.e., $\text{Re} \ll 1$, so that the flow satisfies the Stokes equations.

The typical velocity field in such a channel has been calculated following the method described before [14], and its typical cross section is shown in Fig. 3. Figure 3 illustrates that the transverse velocity is strongly inhomogeneous. The
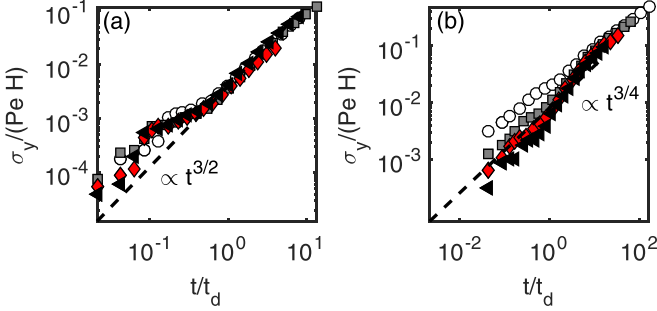
FIG. 4. Dispersion $\sigma_y/(H\mathrm{Pe})$ as a function of time t/t_d simulated for $\phi = 0.5$. The Péclet numbers are (a) Pe $= 200, 300, 400, 500$ (circles, squares, diamonds, triangles) and (b) Pe $= 10, 50, 75, 100$ (circles, squares, diamonds, triangles).
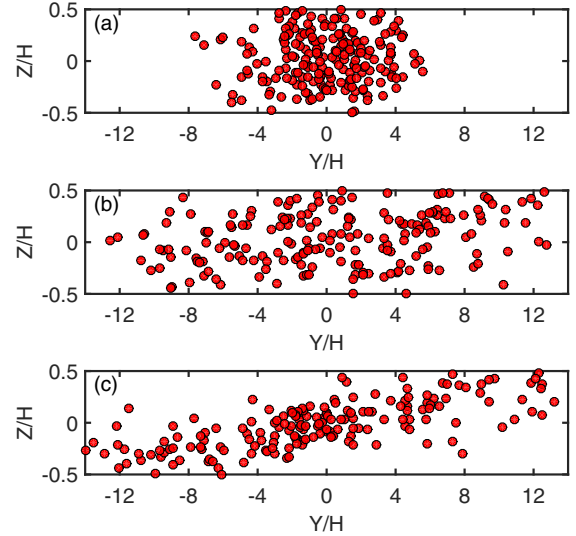

FIG. 5. Positions of individual particles at the cross section $\lambda = 50$ of a SH channel with $\phi = 0.5$. The Péclet number is 10 (a), 50 (b), and 300 (c) providing different scenarios of advective superdiffusion.

inverse average transverse velocity, U_0/U_{sy}, which controls the hydrodynamic dispersion, can be obtained by averaging the three-dimensional velocity field $\mathbf{u}(x,y,z)$ over the periodic cell in the x,y plane. If $H = O(L)$ or larger, it can be evaluated by using a simple expression $U_0/U_{sy} \simeq (1 + 2\beta_+)/(4\beta_-)$, where $\beta_\pm = (b_{\mathrm{eff}}^\parallel \pm b_{\mathrm{eff}}^\perp)/(2H)$ with $b_{\mathrm{eff}}^{\parallel,\perp}$ the eigenvalues of the slip length tensor, $\mathbf{b}_{\mathrm{eff}}$, for a channel of a finite H/L with one SH and one no-slip hydrophilic walls [14]. These eigenvalues have been calculated before [10], and they depend on b, L/H, and ϕ. In our simulations below we use $b = \infty$ since it maximizes the effective slip. We employ $L/H = 2$ since this provides a significant transverse shear [14]. Finally, we consider several textures, with ϕ varying in the interval from $\phi = 0.25$ to 0.9, which with prescribed parameters give a variation of U_0/U_{sy} from $\simeq 11.5$ to 1.2. With these values at moderate Péclet numbers one can expect various regimes of superdiffusion at an appropriate value of λ.

We now inject a large number of Brownian particles in the channel, track their instantaneous positions, and evaluate the dispersion σ_y at a given time. We have first plotted in Fig. 4 the simulation results for $\sigma_y/(\mathrm{Pe}H)$ as a function of t/t_d obtained at $\phi = 0.5$ and several Pe. A general conclusion from this plot is that the above scaling predictions given by Eq. (5) are in good agreement with simulation results. Thus, we see that all curves indeed overlap at long time. For relatively large Péclet numbers, Pe $\geqslant 200$, simulation data confirm the superballistic scaling $(t/t_d)^{3/2}$, but at smaller Péclet numbers, i.e., Pe $\leqslant 100$, our results fully validate the predicted subballistic scaling $(t/t_d)^{3/4}$.

To examine the difference between different advective superdiffusion regimes we now vary Pe at fixed $\phi = 0.5$ and determine positions of individual particles at a given cross section $\lambda = 50$. For this gas area fraction $U_0/U_{sy} \simeq 7.4$, therefore, according to Fig. 2, the values of Pe $= 10, 50$, and 300 should lead to a subballistic regime of superdiffusion, a crossover between subballistic and superballistic regimes, and a superballistic superdiffusion, correspondingly. The simulation results are shown in Figs. 5(a), 5(b), and 5(c). We see that a crossover between subbalistic and superballistic regimes does lead to a homogeneous distribution of particles. A subbalistic regime results in a rather homogeneous distribution of particles by the height of a channel, but σ_y remains small, so that particles are still focused near the midplane of the

channel, $y = 0$. In contrast, in the superballistic regime the particle spreading in the y direction is large, but due to small σ_z the distribution of particles in the cross section is highly inhomogeneous.

Finally, we explore in more details a situation of a maximal transverse hydrodynamic dispersion, $\sigma_{\max}/H$, which occurs when the scaling law

$$\mathrm{Pe}_{\max} \propto \lambda, \qquad (9)$$

is valid. Figure 6(a) shows σ_y/H, versus Pe, calculated at fixed $\phi = 0.75$ and several λ. It can be seen that σ_y/H increases with λ, and that for a given λ there indeed exists a Péclet number, $\mathrm{Pe}_{\max}$, which maximizes the dispersion. Note that the induced by superdiffusion transverse dispersion is large: already at moderate $\lambda = 50$ it could be several times larger than the channel thickness, of course, provided Pe is optimal. The scaling law, Eq. (9), predicts $\mathrm{Pe}_{\max}$ is growing linearly with λ. This is indeed the tendency shown by the simulation results. We now reproduce the data set from Fig. 6(a) in Fig. 6(b), but scale both coordinates by λ. Remarkably, and in agreement with our scaling analysis, simulation data obtained for several
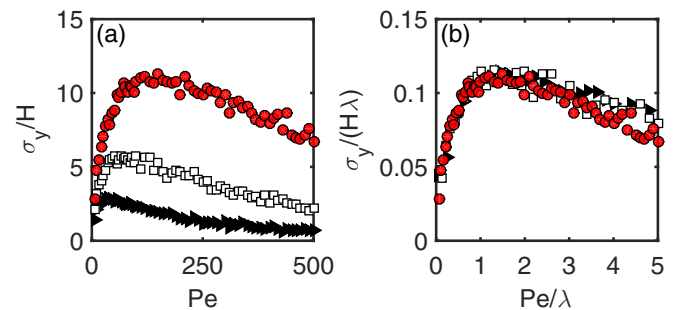

FIG. 6. (a) Transverse particle dispersion σ_y/H as a function of Pe calculated with $\phi = 0.75$ at $\lambda = 25$ (squares), 50 (triangles), and 100 (circles). (b) The same data plotted in scaled by λ coordinates.
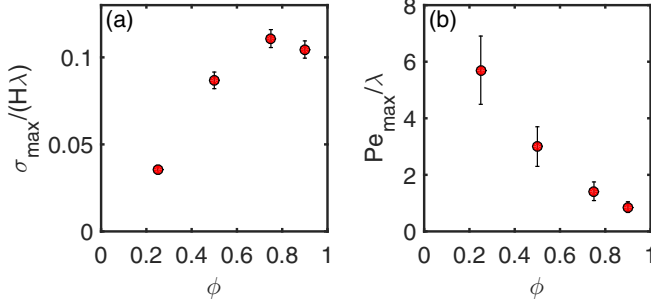
FIG. 7. Rescaled maximal dispersion, $\sigma_{\max}/(H\lambda)$, (a) and the Péclet number, $\mathrm{Pe}_{\max}/\lambda$, (b) as a function of the gas area fraction, ϕ.

λ do collapse into a single curve. This plot allows us to obtain a scaling prefactor in Eq.(9), which for a given $\phi = 0.75$ is found to be $\simeq 1$ (see Appendix A).

Similar curves, $\sigma_y/(H\lambda)$ versus Pe/λ, have been calculated for several gas area fractions, and we have again found that at a given ϕ they nearly coincide (see Appendix A). We have then obtained from these simulation data the values of $\sigma_{\max}/(H\lambda)$ and $\mathrm{Pe}_{\max}/\lambda$ (which gives us exactly the scaling prefactor), and the results are plotted in Fig. 7 as a function of ϕ. A first conclusion emerging from this plot is that ϕ is one of the key parameters determining the maximal value of a transverse dispersion, $\sigma_{\max}/(H\lambda)$. Figure 7(a) shows that in the low ϕ the transverse hydrodynamic dispersion is very small. It grows with the gas area fraction and reaches the maximum at $\phi \simeq 0.75$ (see Appendix B for interpretation of this result). We also note that the scaling prefactor in Eq. (9) decays with ϕ as seen in Fig. 7(b).

Altogether the above simulation results do confirm our simple scaling laws. We can therefore conclude that these expressions provide us with a correct picture of the superdiffusive behavior of particles in the flow, even though they overlook many details.

V. FINAL REMARKS

In conclusion, we believe we have provided a satisfactory answer to several questions posed at the beginning of this paper. We have shown that by using wide microchannels with misaligned striped SH walls it is possible to induce an advective superdiffusion of Brownian particles, which could not be achieved with standard microfluidic devices with smooth walls or in devices which are currently used to enhance mixing at the microscale. We have developed scaling laws for regimes of advective superdiffusion in such a microchannel, providing explicit expressions for mean square displacement of particles as a function of channel thickness and length, Péclet number, and slip velocity at the walls. These scaling results have been validated by means of computer simulations. It has also been shown that the advective superdiffusion could be used to efficiently mix Brownian particles, which is important in a variety of applications.

Certain aspects of our work warrant further comments. A striking conclusion from our work is that the surface textures which optimize $\sigma_{\max}/(H\lambda)$ differ from those optimizing

effective (forward) slip. It is well known that the effective slip of SH surfaces is maximized by increasing the gas-liquid area fraction [4,7,10]. In contrast, we have shown that dispersion of Brownian particles in SH microchannels is maximized by stripes with a smaller gas fraction, $\phi \simeq 0.75$. In this situation, the effective slip is relatively small, and yet the dispersion of particles is very strong.

We should also like to stress that in a bulk or near a single interface the optimal spreading of Brownian particles would obviously occur in a superballistic regime. Our work has shown that that contrary to a bulk situation, maximal cross-sectional spreading at a finite H corresponds to a crossover between subballistic and superballistic regimes of a superdiffusion. Therefore, one can conclude that a superdiffusive behavior of particles in a confined flow is indeed very different from expected for unbounded systems.

Prior work on passive micromixing [18,24] has exploited microchannels of $W/H = O(1)$ and very large Péclet numbers, $\mathrm{Pe} = 10^3$–10^6. This implies that previous methods have been designed to efficiently mix particles of a micron size or slightly smaller. We have addressed a different flow configuration of $W/H \gg 1$, and have argued that an advective superdiffusion can be used for boosting dispersion of particles at much smaller Pe compared to known concepts of passive microfluidic mixing. Our optimal Pe has been found to be of the order of 100 and smaller. This implies that at the same velocities of a mean flow we could provide mixing of particles of the size 10–50 nm (i.e., of truly nanoparticles, including proteins, viruses, etc). Alternatively, our concept allows one mixing of particles of the size of 0.1–1 μm at the same flow rate, $Q = U_0 H W$, but in channels of much smaller H.

APPENDIX A: CALCULATIONS OF OPTIMAL PÉCLET NUMBER AND DISPERSION

To estimate the optimal Péclet number and its dependence on texture parameters we run simulations for several $\lambda = 25, 50, 100$ and several $\phi = 0.25, 0.5, 0.75, 0.9$. The $\sigma_y/(H\lambda)$ versus Pe/λ curves are plotted in Fig. 8. We see that at a given ϕ results for different λ collapse into a single curve. To obtain the position of the maximum we fit these curves to a function

$$f_\sigma = \frac{p_1 x^2 + p_2 x + p_3}{x^2 + p_4 x + p_5}, \tag{A1}$$

where p_i, $i = 1$–5, are the fitting coefficients. To find the best fit for p_i we use the combined data set for all three values of λ. The values $\mathrm{Pe}_{\max}/\lambda$ and $\sigma_{\max}/(H\lambda)$ are then calculated from the fitting function for each ϕ. The error bars in Fig. 7 for the maximal dispersion $\Delta\sigma_{\max}$ are found by estimating the root-mean-square deviation between the fit and the data. The error in $\mathrm{Pe}_{\max}$ is estimated by expanding the fit function around its maximum,

$$\Delta\mathrm{Pe} \sim \sqrt{\Delta\sigma_{\max}/f_\sigma''(\mathrm{Pe}_{\max}/\lambda)}. \tag{A2}$$
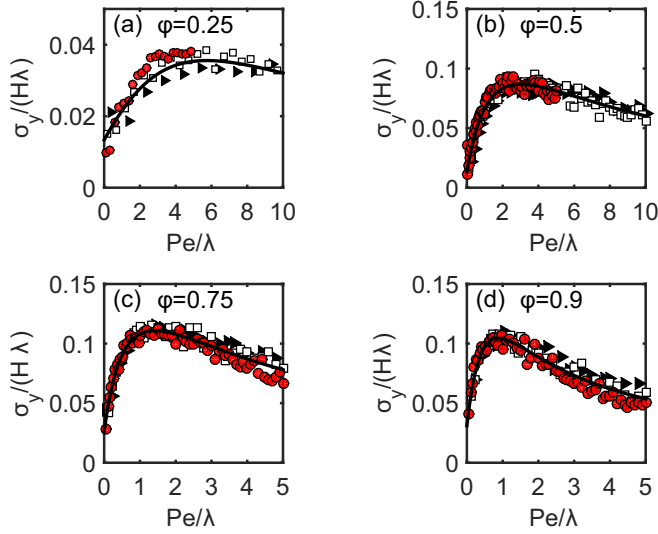
FIG. 8. Particle dispersion σ_y for (a) $\phi = 0.25$, (b) 0.5, (c) 0.75, (d) 0.9 and $\lambda = 25$, 50, 100 (triangles, squares, circles). Solid curves show a fit to f_σ, given by Eq. (A1).

APPENDIX B: THE EFFECT OF LARGE FORWARD SLIP ON THE DISPERSION

The scaling equation (6) has been obtained assuming that the slip velocity at the wall is small compared to that of the Poiseuille flow, $U_{sx}, U_{sy} \ll U_0$, so that they do not include a forward slip U_{sx}. In this appendix, we estimate the contribution of large forward slip, U_{sx}, to σ_y and $\text{Pe}_{\max}$. When U_{sx}, $U_{sy} \simeq U_0$ the mean forward flow velocity is

$$U_m = \begin{cases} U_0 + U_{sx}, & t \ll t_d, \\ 2U_0/3 + U_{sx}, & t \gg t_d. \end{cases}$$

Since $t = \lambda H/U_m$, Eqs. (5) and (6) can be modified to give

$$\frac{\sigma_y^2}{H^2} \propto \begin{cases} \dfrac{\left(U_{sy}/U_0\right)^2 \lambda^3}{(1 + U_{sx}/U_0)^3 \text{Pe}}, & U_0/U_{sy} \ll \lambda \ll \text{Pe}, \\[4mm] \dfrac{\left(U_{sy}/U_0\right)^2 \text{Pe}^{1/2} \lambda^{3/2}}{(2/3 + U_{sx}/U_0)^{3/2}}, & \lambda \gg \text{Pe}, \end{cases}$$

and

$$\frac{\sigma_y^2}{(H\lambda)^2} \propto \begin{cases} \dfrac{\left(U_{sy}/U_0\right)^2}{(1 + U_{sx}/U_0)^3} \text{Pe}/\lambda, & U_0/U_{sy} \ll \lambda \ll \text{Pe}, \\[4mm] \dfrac{\left(U_{sy}/U_0\right)^2}{(2/3 + U_{sx}/U_0)^{3/2}} (\text{Pe}/\lambda)^{1/2}, & \lambda \gg \text{Pe}. \end{cases}$$

When $\phi \to 1$, both U_{sy} and U_{sx} become large, and the dispersion for the first regime decays with ϕ since $\sigma_y^2/H^2 \propto U_0 U_{sy}^2 U_{sx}^{-3}$. However, it grows for the second regime, $\sigma_y^2/H^2 \propto U_0^{1/2} U_{sy}^2 U_{sx}^{-3/2}$. The values of $\text{Pe}_{\max}$ and $\sigma_{\max}$ can be deduced from a crossover between two regimes. Straightforward calculations lead to

$$\text{Pe}_{\max} \simeq \lambda \frac{2/3 + U_{sx}/U_0}{(1 + U_{sx}/U_0)^2} \tag{B1}$$

and

$$\sigma_{\max} \simeq \lambda \frac{U_{sy}/U_0}{(2/3 + U_{sx}/U_0)(1 + U_{sx}/U_0)}. \tag{B2}$$

Therefore, we can conclude that both $\text{Pe}_{\max}$ and $\sigma_{\max}$ decay when $\phi \to 1$, and the maximal dispersion is attained at smaller ϕ.

[1] D. Quere, Rep. Prog. Phys. **68**, 2495 (2005).
[2] T. Darmanin and F. Guittard, J. Mater. Chem. A **2**, 16319 (2014).
[3] L. Bocquet and J. L. Barrat, Soft Matter **3**, 685 (2007).
[4] C. Ybert, C. Barentin, C. Cottin-Bizonne, P. Joseph, and L. Bocquet, Phys. Fluids **19**, 123601 (2007).
[5] J. P. Rothstein, Annu. Rev. Fluid Mech. **42**, 89 (2010).
[6] O. I. Vinogradova and A. L. Dubov, Mendeleev Commun. **22**, 229 (2012).
[7] F. Feuillebois, M. Z. Bazant, and O. I. Vinogradova, Phys. Rev. Lett. **102**, 026001 (2009).
[8] H. A. Stone, A. D. Stroock, and A. Ajdari, Annu. Rev. Fluid Mech. **36**, 381 (2004).
[9] M. Z. Bazant and O. I. Vinogradova, J. Fluid Mech. **613**, 125 (2008).
[10] S. Schmieschek, A. V. Belyaev, J. Harting, and O. I. Vinogradova, Phys. Rev. E **85**, 016324 (2012).
[11] F. Feuillebois, M. Z. Bazant, and O. I. Vinogradova, Phys. Rev. E **82**, 055301(R) (2010).
[12] O. I. Vinogradova and A. V. Belyaev, J. Phys.: Condens. Matter **23**, 184104 (2011).

[13] C. O. Ng and C. Y. Wang, Microfluid Nanofluid **8**, 361 (2010).
[14] T. V. Nizkaya, E. S. Asmolov, J. Zhou, F. Schmid, and O. I. Vinogradova, Phys. Rev. E **91**, 033020 (2015).
[15] C. O. Ng, H. C. W. Chu, and C. Y. Wang, Phys. Fluids **22**, 102002 (2010).
[16] D. Pimponi, M. Chinappi, P. Gualtieri, and C. M. Casciola, Microfluidics Nanofluidics **16**, 571 (2014).
[17] E. S. Asmolov, A. L. Dubov, T. V. Nizkaya, A. J. C. Kuehne, and O. I. Vinogradova, Lab Chip **15**, 2835 (2015).
[18] J. Ou, G. R. Moss, and J. P. Rothstein, Phys. Rev. E **76**, 016304 (2007).
[19] C. Jaimon and S. K. Ranjith, Microsyst. Technol. **23**, 2881 (2017).
[20] E. Frey and K. Kroy, Ann. Phys. **14**, 20 (2005).
[21] Z. Wang, H. Y. Chen, Y. J. Sheng, and H. K. Tsao, Soft Matter **10**, 3209 (2014).
[22] O. I. Vinogradova, K. Koynov, A. Best, and F. Feuillebois, Phys. Rev. Lett. **102**, 118302 (2009).
[23] J. M. Ottino and S. Wiggins, Philos. Trans. A Math. Phys. Eng. Sci. **362**, 923 (2004).

[24] A. D. Stroock, S. K. Dertinger, A. Ajdari, I. Mezić, H. A. Stone, and G. M. Whitesides, Science **295**, 647 (2002).

[25] P. B. Howell Jr, D. R. Mott, F. S. Ligler, J. P. Golden, C. R. Kaplan, and E. S. Oran, J. Micromech. Microeng. **18**, 115019 (2008).

[26] R. Metzler and J. Klafter, Phys. Rep. **339**, 1 (2000).

[27] G. Matheron and G. De Marsily, Water Resour. Res. **16**, 901 (1980).

[28] P. L. Krapivsky, S. Redner, and E. Ben-Naim, *A Kinetic View of Statistical Physics* (Cambridge University Press, Cambridge, 2010).

[29] M. F. Shlesinger, B. J. West, and J. Klafter, Phys. Rev. Lett. **58**, 1100 (1987).

[30] R. T. Foister and T. G. M. Van De Ven, J. Fluid Mech. **96**, 105 (1980).

[31] M. Dentz and B. Berkowitz, Water Resourc. Res. **39**, 1111 (2003).

[32] O. Bénichou, A. Bodrova, D. Chakraborty, P. Illien, A. Law, C. Mejía-Monasterio, G. Oshanin, and R. Voituriez, Phys. Rev. Lett. **111**, 260601 (2013).

[33] T. V. Nizkaya, E. S. Asmolov, and O. I. Vinogradova, Soft Matter **9**, 11671 (2013).